^{18}F-FAC PET Selectively Images Liver-Infiltrating CD4 and CD8 T Cells in a Mouse Model of Autoimmune Hepatitis

Jessica R. Salas[1,2], Bao Ying Chen[1,2], Alicia Wong[1,2], Donghui Cheng[3], John S. Van Arnam[4], Owen N. Witte[1,3,5], and Peter M. Clark[1–3]

[1]Department of Molecular and Medical Pharmacology, UCLA, Los Angeles, California; [2]Crump Institute for Molecular Imaging, UCLA, Los Angeles, California; [3]Eli and Edythe Broad Center of Regenerative Medicine and Stem Cell Research, UCLA, Los Angeles, California; [4]Department of Pathology and Laboratory Medicine, University of Pennsylvania, Philadelphia, Pennsylvania; and [5]Department of Microbiology, Immunology, and Molecular Genetics, UCLA, Los Angeles, California

Immune cell–mediated attack on the liver is a defining feature of autoimmune hepatitis and hepatic allograft rejection. Despite an assortment of diagnostic tools, invasive biopsies remain the only method for identifying immune cells in the liver. We evaluated whether PET imaging with radiotracers that quantify immune activation (^{18}F-FDG and ^{18}F-1-(2′-deoxy-2′-fluoro-arabinofuranosyl)cytosine [^{18}F-FAC]) and hepatocyte biology (^{18}F-2-deoxy-2-fluoroarabinose [^{18}F-DFA]) can visualize and quantify liver-infiltrating immune cells and hepatocyte inflammation, respectively, in a preclinical model of autoimmune hepatitis. **Methods:** Mice treated with concanavalin A (ConA) to induce a model of autoimmune hepatitis or vehicle were imaged with ^{18}F-FDG, ^{18}F-FAC, and ^{18}F-DFA PET. Immunohistochemistry, digital autoradiography, and ex vivo accumulation assays were used to localize areas of altered radiotracer accumulation in the liver. For comparison, mice treated with an adenovirus to induce a viral hepatitis were imaged with ^{18}F-FDG, ^{18}F-FAC, and ^{18}F-DFA PET. ^{18}F-FAC PET was performed on mice treated with ConA and vehicle or with ConA and dexamethasone. Biopsy samples of patients with autoimmune hepatitis were immunostained for deoxycytidine kinase. **Results:** Hepatic accumulation of ^{18}F-FDG and ^{18}F-FAC was 173% and 61% higher, respectively, and hepatic accumulation of ^{18}F-DFA was 41% lower, in a mouse model of autoimmune hepatitis than in control mice. Increased hepatic ^{18}F-FDG accumulation was localized to infiltrating leukocytes and inflamed sinusoidal endothelial cells, increased hepatic ^{18}F-FAC accumulation was concentrated in infiltrating CD4 and CD8 cells, and decreased hepatic ^{18}F-DFA accumulation was apparent in hepatocytes throughout the liver. In contrast, viral hepatitis increased hepatic ^{18}F-FDG accumulation by 109% and decreased hepatic ^{18}F-DFA accumulation by 20% but had no effect on hepatic ^{18}F-FAC accumulation (nonsignificant 2% decrease). ^{18}F-FAC PET provided a noninvasive biomarker of the efficacy of dexamethasone for treating the autoimmune hepatitis model. Infiltrating leukocytes in liver biopsy samples from patients with autoimmune hepatitis express high levels of deoxycytidine kinase, a rate-limiting enzyme in the accumulation of ^{18}F-FAC. **Conclusion:** Our data suggest that PET can be used to noninvasively visualize activated leukocytes and inflamed hepatocytes in a mouse model of autoimmune hepatitis.

Received Feb. 21, 2018; revision accepted Apr. 23, 2018.
For correspondence or reprints contact: Peter M. Clark, Crump Institute, Box 951770, 4333 CNSI, Los Angeles, CA 90095.
E-mail: pclark@mednet.ucla.edu
Guest Editor: Todd Peterson, Vanderbilt University
Published online Apr. 26, 2018.

Key Words: PET imaging; autoimmune disease; hepatitis; hepatocytes

J Nucl Med 2018; 59:1616–1623
DOI: 10.2967/jnumed.118.210328

Immune cell infiltration into the liver and attack on liver cells are characteristic of various diseases, including autoimmune hepatitis and hepatic allograft rejection (*1,2*). Immune-mediated attack on the liver can lead to significant cellular damage, and hepatic allograft rejection is a leading cause of liver retransplantation (*1–4*). T lymphocytes make up a sizable fraction of the liver-infiltrating leukocytes in autoimmune hepatitis and hepatic allograft rejection, and various animal models suggest a critical role for T lymphocytes in these diseases (*5–9*).

Current clinical methods for evaluating hepatocyte inflammation and liver-infiltrating T lymphocytes in vivo are valuable but provide an incomplete picture of disease (*10–17*). Hepatocellular damage can be inferred from blood levels of enzymes and metabolites enriched in or processed by the liver, including alanine transaminase, aspartate transaminase, and bilirubin. However, these measures do not always accurately reflect the degree of liver-infiltrating T lymphocytes and are not predictive of disease reversibility (*10,11*). The liver can also be imaged by CT, MRI, and ultrasound, but these imaging modalities provide limited functional information (*12*). Blood CD4 T-cell intracellular adenosine triphosphate levels, measured ex vivo after stimulation, may provide information on immune activation in the setting of a liver transplant, but the sensitivity and specificity of this approach remain controversial, and this approach provides no direct information on lymphocyte activity specifically in the liver (*13*). Liver biopsies remain the gold standard for assessing liver-infiltrating lymphocytes but suffer significant sampling error, carry a risk of complications, and are often challenging to interpret in diseases with heterogeneous manifestations such as hepatic allograft rejection (*14–17*). A method to selectively quantify and visualize CD4 and CD8 T lymphocytes and inflamed hepatocytes in the liver within the context of autoimmune hepatitis and hepatic allograft rejection could improve our understanding of these diseases and function as a potential biomarker of therapy.

We recently developed a family of PET imaging radiotracers—^{18}F-2-deoxy-2-fluoroarabinose (^{18}F-DFA) and ^{18}F-2-deoxy-2-fluororibose—that measure ribose salvage activity, a pathway highly upregulated in

liver hepatocytes (*18,19*). We showed that ^{18}F-DFA PET quantifies functional hepatocyte density in a mouse model of drug-induced acute liver failure and that hepatic ^{18}F-DFA accumulation is decreased in mouse models of fatty liver disease (*18–20*). Alternatively, the PET radiotracers ^{18}F-FDG and ^{18}F-1-(2′-deoxy-2′-fluoro-arabinofuranosyl) cytosine (^{18}F-FAC) measure glucose consumption and deoxynucleoside salvage, respectively, two processes upregulated during immune cell activation (*21–23*). ^{18}F-FDG and ^{18}F-FAC PET can monitor immune activation in mouse models of systemic autoimmune disease, colitis, and immune-mediated tumor rejection (*22–26*). Consistent with studies indicating that PET can be used to image autoimmune disease in other organ systems (*27–29*), previous studies suggest that hepatic ^{18}F-FDG accumulation is increased in a mouse model of autoimmune hepatitis and a rat model of hepatic allograft rejection (*30,31*), although the precise cellular source of this increased accumulation remains unclear.

Here, we study ^{18}F-FDG, ^{18}F-FAC, and ^{18}F-DFA in mouse models of autoimmune and viral hepatitis. ^{18}F-DFA instead of ^{18}F-2-deoxy-2-fluororibose was chosen here because ^{18}F-DFA can be synthesized on an automated radiosynthesizer and its radiochemical precursor is commercially available (*32*). Our results suggest that PET imaging with radiotracers that measure ribose and deoxynucleoside salvage can be used to image and quantify hepatocyte inflammation and liver-infiltrating T lymphocytes during autoimmune hepatitis.

MATERIALS AND METHODS

Mice

Male BALB/c (8–10 wk old) and nonobese diabetic *scid*-γ (NSG; Jackson Laboratory) (8–10 wk old) mice were used for the concanavalin A (ConA) experiments. Male FVB (8–10 wk old) and NSG (8–10 wk old) mice were used for the adenovirus experiments. BALB/c and NSG mice were from an internal UCLA mouse breeding colony. FVB mice were from the Jackson Laboratory. All animal experiments were approved in advance by the UCLA Animal Research Committee.

Treatments

ConA. Mice were injected intravenously with saline vehicle or ConA (type IV, 10 mg/kg; Sigma-Aldrich).

Adenovirus. Mice were injected intravenously and intraperitoneally with a green fluorescent protein–expressing adenovirus (100 μL each; titer, 5×10^8 plaque-forming units/mL; Cyagen).

Dexamethasone. Mice were injected with 1× phosphate-buffered saline vehicle or dexamethasone-21-phosphate (300 mg/kg) intraperitoneally 18 and 1 h before the ConA injection.

Immunohistochemical Analyses

Immunohistochemistry was performed as previously described (*20*) with the following exceptions: antigen retrieval was performed in citrate antigen retrieval buffer (10 mM sodium citrate, pH 6.0) for deoxycytidine kinase (dCK), glucose transporter 1 (GLUT1), CD4, CD8, CD11b, and Ki-67 or a citrate-polysorbate 20 antigen retrieval buffer (10 mM sodium citrate, 0.05% polysorbate 20, pH 6.0) for B220. The slides were blocked in 2.5% horse serum (1 h at room temperature for GLUT1, CD8, B220, CD11b, and Ki-67 or overnight at 4°C for CD4) and incubated with primary antibody (overnight at 4° C for GLUT1, CD8, B220, CD11b, and Ki-67 or 1 h at room temperature for CD4; diluted in 2.5% horse serum). Antibodies and dilutions were as follows: dCK (clone 9D4; 1:1,000; developed by the Witte Lab), GLUT1 (clone 07-1401; 1:500; Millipore), CD4 (ab183685; 1:200; Abcam), CD8 (clone 4SM15; 1:200; eBiosciences), B220 (clone RA3-6B2; 1:100; Biolegend), CD11b (ab75476; 1:1,000; Abcam), and Ki-67 (ab16667; 1:1,000; Abcam). The slides were washed in 1× phosphate-buffered saline and incubated with horse antirabbit horseradish peroxidase (1 h at room temperature for GLUT1, CD4, CD11b, and Ki-67; Vector Laboratories) or treated with Elite ABC complex following the manufacturer's protocol (PK-6100, for B220 and CD8; Vector Laboratories).

Liver sections from anonymized patients with autoimmune hepatitis were obtained from banked biopsy samples through the UCLA Translational Pathology Core Laboratory.

PET/CT Imaging and Quantification

PET imaging and quantification were performed as previously described (*20*). Briefly, anesthetized mice were injected with approximately 2.96 MBq (for the ConA experiments) or approximately 0.74 MBq (for the adenovirus experiments) and imaged 1 h later by PET/CT for 10 min on a G8 PET/CT system (Sofie Biosciences). ^{18}F-FDG was from the UCLA Translational Imaging Division. ^{18}F-FAC and ^{18}F-DFA were synthesized as previously described (*32*). The mice were injected with tracer approximately 30 h after the ConA treatment and were imaged 1–3 d before and then again 2, 4, 8, and 12 wk after the adenovirus injections. Quantified PET images are reported as signal-to-background ratio, where signal refers to radiotracer accumulation in the liver and background refers to radiotracer accumulation in a background organ (^{18}F-FDG: right forelimb triceps; ^{18}F-FAC and ^{18}F-DFA: brain).

Autoradiography

Autoradiography was performed as previously described (*20*). Frozen slides were fixed, stained with hematoxylin and eosin, and digitally imaged.

Ex Vivo Accumulation Assays

The mice were treated with ConA as described above. Liver-infiltrating leukocytes were isolated, sorted, and treated as previously described (*24,33*) except that the radiotracer ^{3}H-deoxycytidine (Moravek, Inc.) was used.

Statistical Analysis

Data are plotted as mean, with error bars representing SEM. Statistical analyses were performed using 1-way and 2-way ANOVA with Tukey and Dunnett corrections, respectively, for multiple comparisons. Statistical analyses were performed by GraphPad Prism (version 7.01).

RESULTS

Hepatic ^{18}F-FDG, ^{18}F-FAC, and ^{18}F-DFA Accumulation Is Affected in a Mouse Model of Autoimmune Hepatitis

The best-studied mouse model of autoimmune hepatitis is induced by treating mice with the plant lectin ConA (*9*). When injected into mice, ConA produces a CD4 T-cell– and tumor necrosis factor-α–dependent but CD8 T-cell–independent hepatitis (*9,34*). Mice injected with ConA exhibited a robust, periportal hepatitis, characterized by liver-infiltrating leukocytes containing a high proportion of CD4 T cells (64% ± 2%), with additional contributions from CD11b-positive innate immune cells, B220-positive B cells, and CD8 T cells (9% ± 2%, 18% ± 2%, and 13% ± 1%, respectively; Fig. 1A). A sizable fraction of the liver-infiltrating leukocytes expressed Ki-67 (67% ± 4%; Fig. 1A), a marker of cell proliferation. In agreement with the literature (*30*), mice treated with ConA had a significantly higher accumulation of hepatic ^{18}F-FDG than did saline vehicle–treated mice (Figs. 1B and 1C; Supplemental Fig. 1). Mice treated with ConA also exhibited higher levels of hepatic ^{18}F-FAC accumulation and lower levels of hepatic ^{18}F-DFA accumulation than vehicle-treated mice (Figs. 1B and 1C; Supplemental Fig. 1).

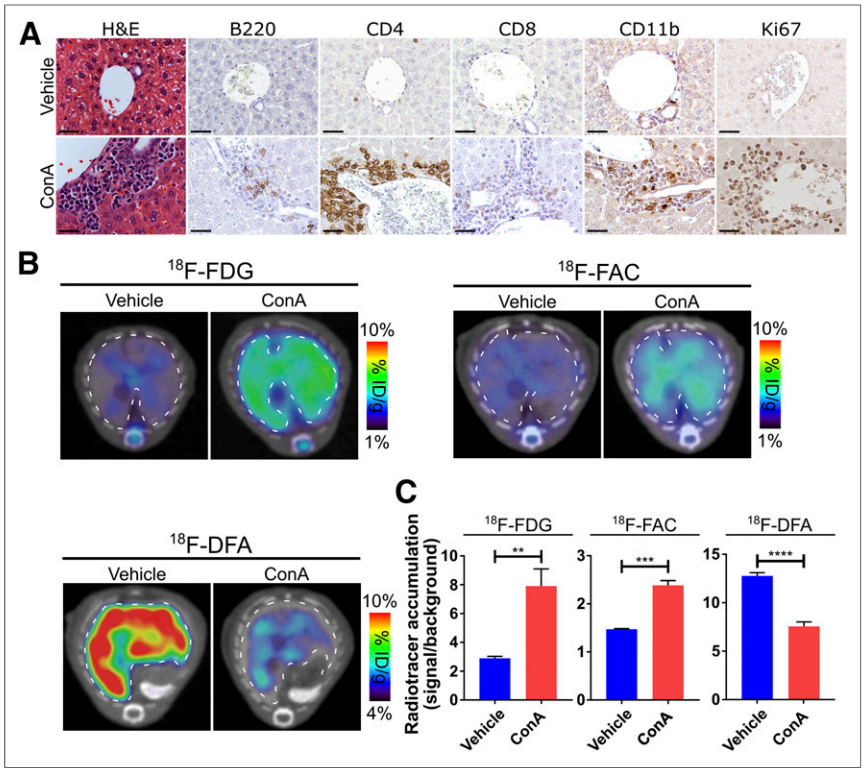

FIGURE 1. Hepatic ^{18}F-FDG, ^{18}F-FAC, and ^{18}F-DFA accumulation is affected in mouse model of autoimmune hepatitis. (A) Histochemical and immunohistochemical analyses of liver sections from vehicle- and ConA-treated mice. Scale bars represent 50 μm. (B and C) Transverse PET/CT images (B) and quantification (C) of vehicle- and ConA-treated mice injected with ^{18}F-FDG, ^{18}F-FAC, and ^{18}F-DFA. Livers are outlined. Quantification represents radiotracer accumulation in liver normalized to background organ. $^{**}P < 0.01$. $^{***}P < 0.001$. $^{****}P < 0.0001$. H&E = hematoxylin and eosin; ID = injected dose.

Consistent with a functional role for the immune system in ConA-induced hepatitis (*9*), liver sections from immunocompromised NSG mice treated with ConA were indistinguishable histologically or immunohistochemically from liver sections of control mice (Supplemental Fig. 2A). No difference in hepatic ^{18}F-FDG, ^{18}F-FAC, or ^{18}F-DFA accumulation was observed between vehicle- and ConA-treated immunocompromised mice (Supplemental Figs. 2B and 2C; Supplemental Fig. 1), indicating that the changes we observed in hepatic tracer accumulation in the immunocompetent mice were due to the ConA-induced hepatitis and were not unrelated effects of the ConA treatment.

Liver-Infiltrating CD4 T Cells Are a Major Source of Increased Hepatic ^{18}F-FAC Accumulation in ConA-Induced Autoimmune Hepatitis

To better understand why hepatic ^{18}F-FDG, ^{18}F-FAC, and ^{18}F-DFA accumulation is affected in ConA-induced autoimmune hepatitis, we studied the system at a cellular level. The cellular accumulation of ^{18}F-FDG, ^{18}F-FAC, and ^{18}F-DFA is regulated by specific proteins (*18,35,36*), and changes in the levels of these proteins in the liver could in part explain changes in hepatic radiotracer accumulation. Expression and membrane localization of the facilitative glucose transporter GLUT1 is a major determinant of glucose consumption in activated lymphocytes, dCK regulates the cellular accumulation of ^{18}F-FAC, and ribokinase is a key enzyme in the ribose salvage pathway that ^{18}F-DFA measures (*36–38*).

Liver sections from ConA-treated mice immunostained for GLUT1 showed high levels of membrane-localized GLUT1 in liver-infiltrating leukocytes, as well as increased GLUT1 membrane expression in leukocyte-proximal liver sinusoidal endothelial cells (Fig. 2A). Ribokinase protein levels were absent from liver-infiltrating leukocytes but present at high levels in liver hepatocytes (Fig. 2A). Liver-infiltrating leukocytes in ConA-treated mice expressed high dCK protein levels, and hepatocyte dCK levels were similar between vehicle and ConA-treated mouse liver sections (Fig. 2A). GLUT1, ribokinase, and dCK protein levels were unaffected in the livers of ConA-treated compared with vehicle-treated immunocompromised mice (Supplemental Fig. 3).

Autoradiography results of liver sections from vehicle- or ConA-treated mice injected with ^{18}F-FDG, ^{18}F-FAC, or ^{18}F-DFA were coregistered with images of these same sections stained with hematoxylin and eosin. Areas of increased ^{18}F-FDG and ^{18}F-FAC accumulation, measured by autoradiography, were coincident with areas of significant leukocyte infiltration (Fig. 2B), suggesting that liver-infiltrating leukocytes are a major source of the increased hepatic ^{18}F-FDG and ^{18}F-FAC accumulation identified in ConA-treated mice. Regions of increased autoradiographic signal were 2.8-fold larger in the ConA-treated mice injected with ^{18}F-FDG than in the ConA-treated mice injected with ^{18}F-FAC ($P < 0.0001$). This finding may indicate that ^{18}F-FAC is more specific than ^{18}F-FDG for liver-infiltrating leukocytes, and is consistent with the immunohistochemistry results (Fig. 2A). ^{18}F-DFA accumulation was decreased throughout the liver in ConA-treated mice and was not coincident with regions of significant leukocyte infiltration (Fig. 2B), consistent with decreased ribose salvage activity in hepatocytes throughout the liver. These data suggest that in ConA-treated mice, liver-infiltrating leukocytes consume high levels of ^{18}F-FAC, that hepatic infiltration leukocytes and nearby liver sinusoidal endothelial cells consume high levels of ^{18}F-FDG, and that inflamed hepatocytes decrease their ^{18}F-DFA accumulation.

Given the potential specificity of ^{18}F-FAC for liver-infiltrating leukocytes, the further selectivity of ^{18}F-FAC for specific leukocyte populations was analyzed. A previous study demonstrated that during immune-mediated tumor rejection, ^{18}F-FAC preferentially accumulated in adaptive immune cells (*24*). Our immunohistochemistry data suggest that CD4-, CD8-, B220-, and CD11b-positive leukocytes all infiltrate into the liver in the ConA-treated mice (Fig. 1A). CD4-, CD8-, B220-, and CD11b-positive cells were isolated from the liver of ConA-treated mice and incubated with ^{3}H-deoxycytidine to measure deoxynucleoside salvage activity. Per cell, CD4 and CD8 T cells consumed approximately 4-fold more deoxycytidine than B220 or CD11b cells (Fig. 2C), and CD4 T cells were present in higher numbers than CD8 T cells in ConA-treated livers (Fig. 1A). Collectively, these data suggest that increased hepatic ^{18}F-FAC accumulation predominantly measures infiltrating CD4 cells in the livers of ConA-treated mice.

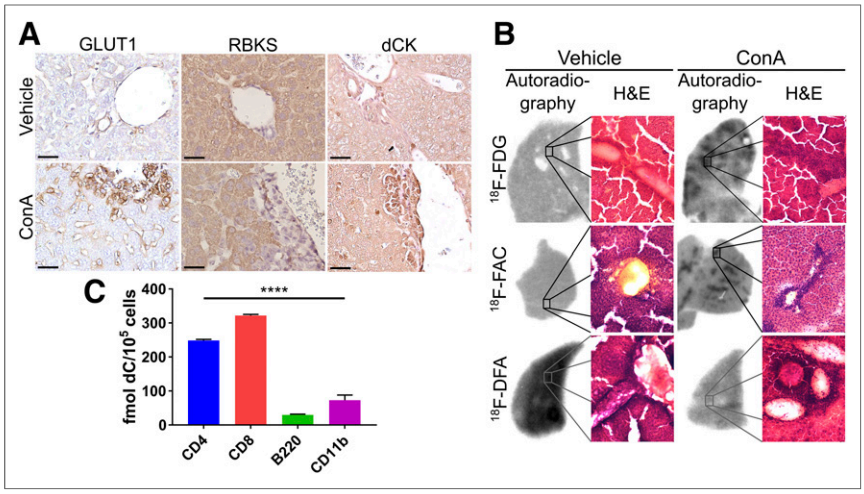

FIGURE 2. ^{18}F-FDG and ^{18}F-FAC measure liver-infiltrating leukocytes, and ^{18}F-DFA measures hepatocyte inflammation. (A) GLUT1, ribokinase, and dCK immunostained vehicle- and ConA-treated mouse liver sections. Scale bars represent 50 μm. (B) Autoradiographic and histologic analyses of liver sections from vehicle- and ConA-treated mice injected with ^{18}F-FDG, ^{18}F-FAC, or ^{18}F-DFA. (C) Ex vivo accumulation of deoxycytidine in sorted leukocytes from livers of ConA-treated mice. $^{****}P < 0.0001$. H&E = hematoxylin and eosin; RBKS = ribokinase.

Hepatic Accumulation of ^{18}F-FDG and ^{18}F-DFA But Not ^{18}F-FAC Is Affected by Viral Hepatitis

Autoimmune hepatitis is one, but not the only, condition characterized by immune cell infiltration into the liver. Histologically, viral hepatitis closely resembles autoimmune hepatitis. We studied the behavior of ^{18}F-FDG, ^{18}F-FAC, and ^{18}F-DFA in a model of viral hepatitis. Viral hepatitis was induced by treating mice with a replication-defective green fluorescent protein–expressing adenovirus. Immunocompromised NSG mice were used to control for non–immune-related effects of the adenoviral treatment on radiotracer accumulation. Mice treated with the adenovirus mount a robust immune attack on the liver within 2 wk of treatment that persists through 8 wk before clearing by 12 wk, leaving only histiocytes as evidence of the antecedent inflammation (Fig. 3A). Within the periportal leukocyte infiltrates, a significant proportion of the cells consisted of CD4 T cells and CD11b-positive innate immune cells whereas a smaller proportion of the cells consisted of B220-positive B cells and CD8-positive T cells (36% ± 2%, 47% ± 4%, 10% ± 2%, and 11% ± 2%, respectively). A smaller fraction of the infiltrating leukocytes was Ki-67–positive than in the autoimmune hepatitis model (37% ± 3% for this model vs. 67% ± 4% for the autoimmune hepatitis model; Figs. 1A and 3A). At the level of histology and immunohistochemistry, the livers of the immunocompromised mice were largely unaffected by the viral treatment (Supplemental Fig. 4A).

Similar to results obtained in the autoimmune hepatitis model, viral hepatitis induced a significant increase in hepatic ^{18}F-FDG accumulation that returned to pretreatment levels after the hepatitis resolved (Figs. 3B and 3C; Supplemental Fig. 5). Viral hepatitis also decreased hepatic ^{18}F-DFA accumulation, which returned to higher than baseline levels at 12 wk after treatment (Figs. 3B and 3C; Supplemental Fig. 5). We speculate that hepatic ^{18}F-DFA accumulation is elevated at 12 wk after treatment because of a compensatory response of the liver hepatocytes to the prior decrease in hepatic ^{18}F-DFA accumulation. In contrast to the results from the autoimmune hepatitis model (Figs. 1B and 1C), hepatic ^{18}F-FAC accumulation was unaffected at any time point throughout the induction and clearance of the viral hepatitis (Figs. 3B and 3C; Supplemental Fig. 5). No change in hepatic ^{18}F-FDG, ^{18}F-DFA, or ^{18}F-FAC accumulation was identified in immunocompromised mice treated with adenovirus, suggesting that the above results required immune activation (Supplemental Figs. 4B, 4C, and 5).

Changes in Hepatic ^{18}F-FAC Accumulation Can Be Used to Monitor Immunosuppressive Drug Treatments in a Mouse Model of Autoimmune Hepatitis

One potential application for a PET strategy that can quantify liver-infiltrating CD4 and CD8 T lymphocytes is monitoring the response of these cells to immunosuppressive therapies, similar to the role of PET in other fields, including oncology (*39*). Studies suggest, and we found, that pretreatment of mice with the immunosuppressive drug dexamethasone can block ConA-induced autoimmune hepatitis (Fig. 4A) (*9*). Mice treated with dexamethasone 18 and 1 h before treatment with ConA had significantly lower levels of hepatic ^{18}F-FAC accumulation than mice treated with ConA and vehicle (Figs. 4B and 4C). This finding suggests that PET imaging with ^{18}F-FAC can be used as a biomarker for immunomodulatory therapies developed to treat autoimmune hepatitis.

Liver-Infiltrating Leukocytes in Patients with Autoimmune Hepatitis Express dCK

Our data suggest that ^{18}F-FAC may selectively image CD4 and CD8 T cells during autoimmune hepatitis. Whether this is true in humans remains to be determined and is the basis for future studies. To assess deoxynucleoside salvage activity in liver-infiltrating leukocytes in human patients with autoimmune hepatitis, we immunostained tissue sections from biopsy samples of patients with autoimmune hepatitis for dCK. Liver-infiltrating leukocytes in these liver sections stained strongly for dCK (Fig. 5), providing early evidence that PET tracers that measure dCK activity can potentially be used to quantify liver-infiltrating lymphocytes in humans with autoimmune hepatitis.

DISCUSSION

In our studies, ^{18}F-FAC selectively accumulates in the autoimmune but not viral hepatitis model. Hepatic ^{18}F-FDG and ^{18}F-DFA accumulation was affected to a similar extent in the autoimmune and viral hepatitis models, suggesting that the difference in ^{18}F-FAC accumulation between the two models is not due solely to differences in the magnitude of the immune response. Determining the precise mechanism for the selectivity of ^{18}F-FAC for autoimmune over viral hepatitis is beyond the scope of this work. However, previous studies suggest a strong correlation between ^{18}F-FAC accumulation and cell cycle in immune cells (*24*). The ConA-induced autoimmune hepatitis model has faster kinetics than the viral hepatitis model. ConA induces autoimmune hepatitis within 24 h of injection that begins to clear by 48 h. The viral

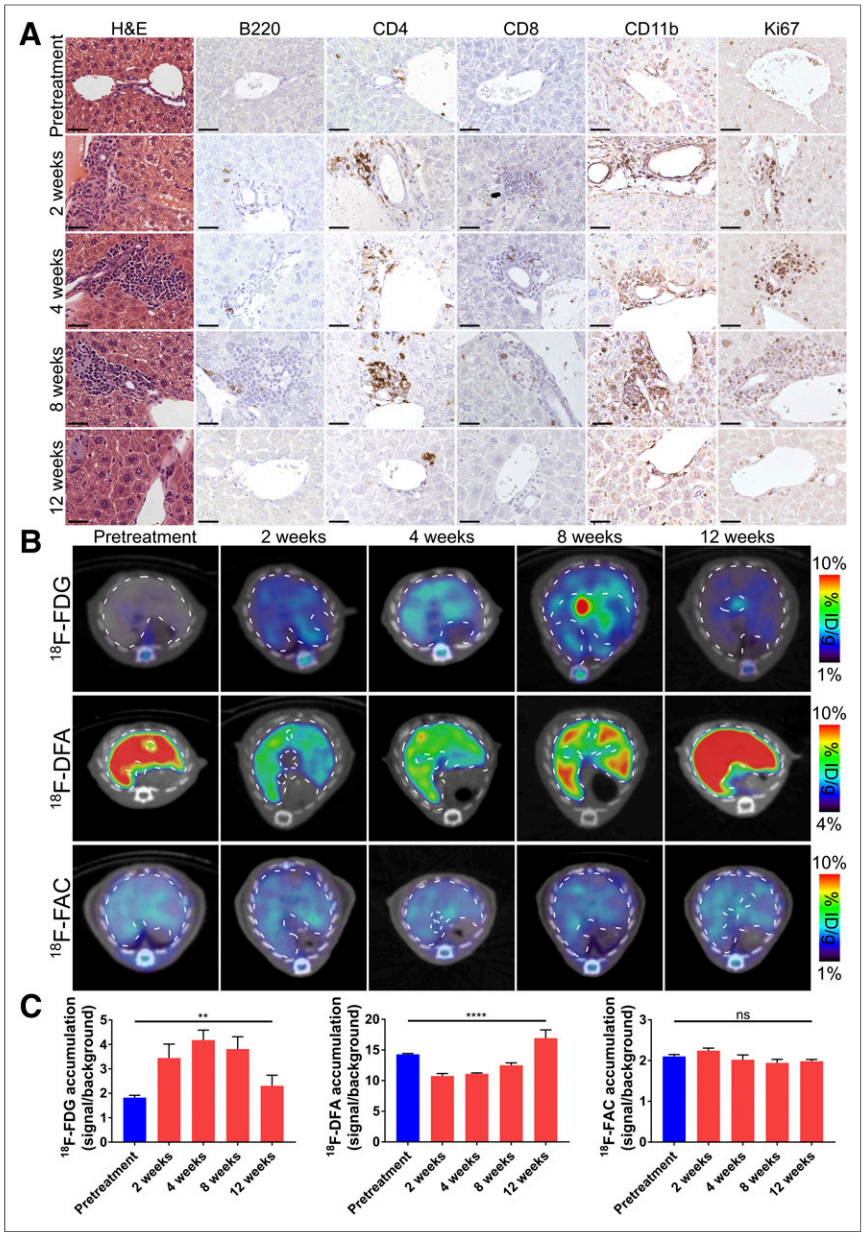

FIGURE 3. Hepatic accumulation of ^{18}F-FDG and ^{18}F-DFA but not ^{18}F-FAC is affected in mouse model of viral hepatitis. (A) Histochemical and immunohistochemical analyses of liver sections from pretreatment and adenovirus-treated mice. Scale bars represent 50 μm. (B and C) Transverse PET/CT images (B) and quantification (C) of pretreatment and adenovirus-treated mice injected with ^{18}F-FDG, ^{18}F-DFA, and ^{18}F-FAC. Quantification represents radiotracer accumulation in liver normalized to background organ. $^{**}P < 0.01$. $^{****}P < 0.0001$. H&E = hematoxylin and eosin; ID = injected dose; ns = not significant.

hepatitis is induced within 2 wk and takes 12 wk to clear. Consistent with these kinetics, a higher percentage of liver-infiltrating leukocytes is positive for the cellular proliferation marker Ki-67 in the ConA-induced autoimmune hepatitis model than in the viral hepatitis model (67% ± 4% vs. 37% ± 3%, respectively; Figs. 1A and 3A). Additionally, we showed high deoxynucleoside salvage activity in CD4 T cells in the autoimmune hepatitis model, and this model has a higher percentage of CD4 T cells among the liver-infiltrating leukocytes than did the viral hepatitis model (64% ± 2% vs. 36% ± 2%, respectively). This finding may suggest that ^{18}F-FAC accumulates in liver-infiltrating lymphocytes in the ConA-induced autoimmune hepatitis model because of a greater percentage of CD4 cells and greater cell proliferation among the infiltrating immune cells in this model.

We found that hepatic ribose salvage activity is decreased uniformly throughout liver hepatocytes in both the autoimmune and the viral hepatitis models and is not localized to areas of significant leukocyte infiltration. Little is known about the regulation of ribose salvage activity. However, the fact that ribose salvage is affected in hepatocytes adjacent to and distant from the infiltrating immune cells suggests a potential role for cytokines in this process. Previous studies reported that during ConA-induced autoimmune hepatitis, plasma protein and liver messenger RNA levels of cytokines, including tumor necrosis factor, IFN-γ, IL-2, IL-4, IL-6, IL-10, and IL-12, are all elevated (*40*). Whether cytokines regulate ribose salvage activity in this model remains to be determined.

Our studies suggest that deoxynucleoside salvage activity in the liver, measured by ^{18}F-FAC accumulation, is higher in a mouse model of autoimmune hepatitis than in control mice. dCK is a rate-limiting enzyme for deoxynucleoside salvage (*36*). The precise role of deoxynucleoside salvage in T-cell activation is not well described, but genetic inactivation of dCK in mice blocks lymphocyte development and leads to significantly lower lymphocyte numbers (*36*). Recently, small-molecule inhibitors of dCK have been developed (*41*). Although further studies are required, our results may suggest new therapeutic opportunities for targeting dCK in the context of autoimmune hepatitis.

Implications for Human Studies

Diagnosing autoimmune hepatitis and hepatic allograft rejection and monitoring therapeutic responses in these diseases remain a challenge (*42–44*). In routine clinical practice, autoimmune hepatitis is diagnosed through descriptive criteria with consideration of features such as liver histology and serum biochemistries. A semiquantitative scoring system used in clinical trials that attributes positive or negative points to the presence or absence of alterations in liver histology, serum biochemistry, and serum autoantibodies improves on the descriptive criteria (*1*). Similarly, hepatic allograft rejection is diagnosed through a combination of liver biochemistry measurements and histologic features (*2*). All of these approaches depend on interpreting the results of a liver biopsy, which can be subject to significant sampling and reader error and is not without risk (*14–17*). We hypothesize that PET imaging with ^{18}F-FAC (or ^{18}F-FAC

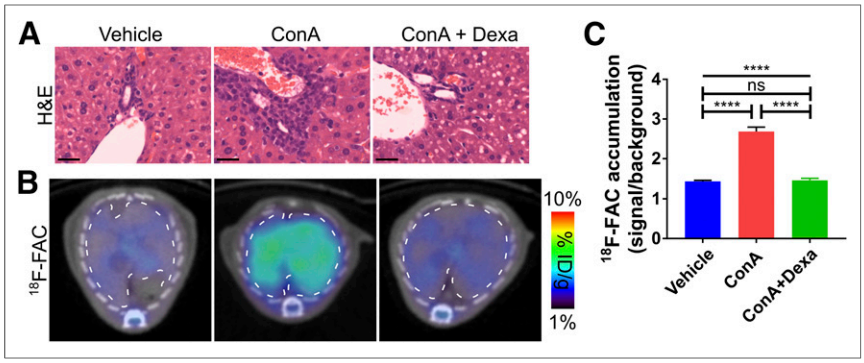

FIGURE 4. Changes in hepatic ^{18}F-FAC accumulation can be used to monitor immunosuppressive drug treatments in mouse model of autoimmune hepatitis. (A) Representative hematoxylin- and eosin-stained liver sections of mice treated with vehicle, ConA, or ConA and dexamethasone. Scale bars represent 50 μm. (B) Transverse PET/CT images of hepatic ^{18}F-FAC accumulation in mice treated with vehicle, ConA, or ConA and Dexa. (C) Quantification of hepatic ^{18}F-FAC accumulation in mice treated with vehicle, ConA, or ConA and Dexa. Quantification represents radiotracer accumulation in liver normalized to background organ. ****$P < 0.0001$. Dexa = dexamethasone; H&E = hematoxylin and eosin; ID = injected dose; ns = not significant.

derivatives) can provide a tomographic, whole-organ, quantitative assessment of activated liver-infiltrating lymphocytes in these diseases and can complement biopsies. ^{18}F-DFA PET might provide the same with respect to the presence of inflamed hepatocytes.

Autoimmune hepatitis and hepatic allograft rejection are treated with immunosuppressive drugs (*1,2*). These therapies are often effective but have narrow therapeutic windows, significant side effects, and high patient-to-patient variability in their pharmacokinetics and pharmacodynamics (*45,46*). Without a method for quantifying activated immune cells in the liver, identifying the correct dose of an immunosuppressive drug for an individual patient that blocks immune attack on the liver while limiting unwanted side effects remains a significant clinical challenge (*47*). The ability to directly and quantitatively measure liver-infiltrating lymphocytes—a desired target of these immunomodulatory drugs—could serve as a valuable biomarker for assessing efficacy.

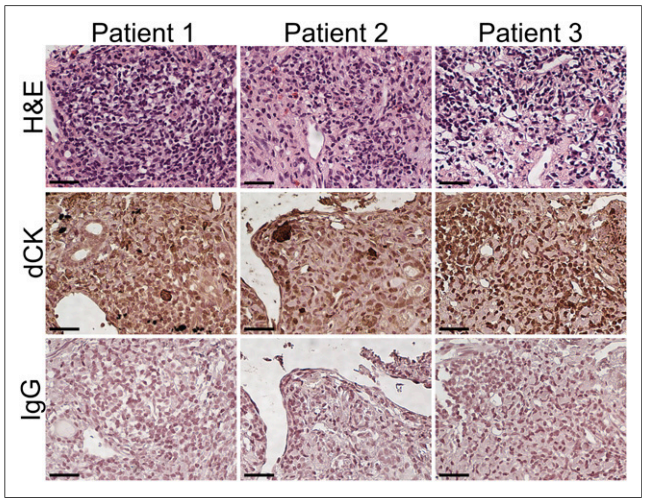

FIGURE 5. Liver-infiltrating leukocytes in patients with autoimmune hepatitis express dCK. Histochemical and immunohistochemical analyses of liver biopsies from patients with autoimmune hepatitis. Scale bars represent 50 μm. H&E = hematoxylin and eosin.

Here, we show in a mouse model that ^{18}F-FAC PET can quantitatively assess liver-infiltrating lymphocytes and can be used to monitor the efficacy of an immunomodulatory drug.

The most prevalent hepatitis-inducing viruses in humans are hepatitis B and C. These diseases can occur as acute infections that resolve or can persist as chronic infections (*48*). Insofar as the adenovirus infection in mice resolves, it models an acute rather than a chronic infection. The lack of any effect on hepatic radiotracer accumulation in the adenovirus-treated immunocompromised mice suggests that the effects identified in the adenovirus-treated immunocompetent mice are solely due to immune attack on the liver and not to the adenovirus infection by itself. Chronic hepatitis infections are characterized by exhausted and impaired immune cell responses to the virus, an immunologic state associated with decreased glucose consumption (*48,49*). We would have to study a chronic hepatitis model to understand the behavior of the radiotracers during a chronic infection. However, we can speculate that the differences we identify here in hepatic ^{18}F-FDG and ^{18}F-DFA accumulation during the adenoviral infection would likely be muted during a chronic infection.

In a recent study, we showed that ribose salvage activity, the biochemical pathway measured by ^{18}F-DFA, is similar between mouse and human hepatocytes in culture and when engrafted into a mouse liver (*20*). This finding suggests that the ^{18}F-DFA imaging results presented here may be translatable into human studies.

^{18}F-FAC images dCK activity in mice but is subject to deamination by the enzyme cytidine deaminase (*50*). Cytidine deaminase activity is higher in most human tissues than in mouse tissues, and ^{18}F-FAC accumulation in lymphoid organs such as the spleen is lower in humans than in mice (*24,51,52*). ^{18}F-FAC accumulation is also low in the human liver (*52*). The PET radiotracer 2-chloro-2′-deoxy-2′-^{18}F-fluoro-9-D-arabinofuranosyl-adenine is a substrate for dCK and resistant to deamination by cytidine deaminase (*53*). This radiotracer accumulates at high levels in lymphoid organs in humans but also at high levels in the healthy human liver (*54*), and high accumulation in the healthy liver would disfavor its use for imaging lymphocytes in the human liver. However, whether activated human CD4 and CD8 T cells could accumulate sufficient ^{18}F-FAC in the setting of high intracellular and peripheral cytidine deaminase activity to produce a PET image remains to be determined.

CONCLUSION

Our results suggest that PET imaging can potentially provide a quantitative, noninvasive method for monitoring hepatocytes and liver-infiltrating T cells during autoimmune hepatitis and in response to therapy. Previous studies suggest that ^{18}F-FAC can be used to visualize a mouse model of systemic autoimmunity and colitis (*23,26*). The value with respect to treatment would be in directly assessing the targets of disease-modifying therapies. Collectively, these studies begin to suggest a potential role for

^{18}F-FAC PET and PET tracers with organ-specific accumulation to visualize and quantify the development and treatment of autoimmune diseases.

DISCLOSURE

This work was supported by NIH grant R21AI119916 (to Peter Clark), Parker Institute for Cancer Immunotherapy (PICI) grant 20163828 (to Owen Witte), and the Broad Stem Cell Research Center at UCLA. Peter Clark and Owen Witte are inventors on a patent, held by the Regents of the University of California, that describes the ^{18}F-DFA radiotracer. No other potential conflict of interest relevant to this article was reported.

ACKNOWLEDGMENTS

We thank the UCLA Translational Pathology Core Laboratory, the Crump Preclinical Imaging Technology Center, and the Crump Cyclotron and Radiochemistry Technology Center for assisting in these studies. We thank Ralph and Marjorie Crump for their gift to the UCLA Crump Institute for Molecular Imaging.

REFERENCES

1. Manns MP, Czaja AJ, Gorham JD, et al. Diagnosis and management of autoimmune hepatitis. *Hepatology.* 2010;51:2193–2213.
2. Batts KP. Acute and chronic hepatic allograft rejection: pathology and classification. *Liver Transpl Surg.* 1999;5(suppl):S21–S29.
3. Rosen HR. Transplantation immunology: what the clinician needs to know for immunotherapy. *Gastroenterology.* 2008;134:1789–1801.
4. Markmann JF, Markowitz JS, Yersiz H, et al. Long-term survival after retransplantation of the liver. *Ann Surg.* 1997;226:408–418, discussion 418–420.
5. Senaldi G, Portmann B, Mowat AP, Mieli-Vergani G, Vergani D. Immunohistochemical features of the portal tract mononuclear cell infiltrate in chronic aggressive hepatitis. *Arch Dis Child.* 1992;67:1447–1453.
6. McCaughan GW, Davies JS, Waugh JA, et al. A quantitative analysis of T lymphocyte populations in human liver allografts undergoing rejection: the use of monoclonal antibodies and double immunolabeling. *Hepatology.* 1990;12:1305–1313.
7. Li W, Lu L, Wang Z, et al. Il-12 antagonism enhances apoptotic death of T cells within hepatic allografts from Flt3 ligand-treated donors and promotes graft acceptance. *J Immunol.* 2001;166:5619–5628.
8. Qian S, Lu L, Fu F, et al. Apoptosis within spontaneously accepted mouse liver allografts: evidence for deletion of cytotoxic T cells and implications for tolerance induction. *J Immunol.* 1997;158:4654–4661.
9. Tiegs G, Hentschel J, Wendel AA. T cell-dependent experimental liver injury in mice inducible by concanavalin A. *J Clin Invest.* 1992;90:196–203.
10. Czaja AJ, Wolf AM, Baggenstoss AH. Laboratory assessment of severe chronic active liver disease during and after corticosteroid therapy: correlation of serum transaminase and gamma globulin levels with histologic features. *Gastroenterology.* 1981;80:687–692.
11. Czaja AJ, Ludwig J, Baggenstoss AH, Wolf A. Corticosteroid-treated chronic active hepatitis in remission: uncertain prognosis of chronic persistent hepatitis. *N Engl J Med.* 1981;304:5–9.
12. Grunwald D, Kothari D, Malik R. Noninvasive markers in the assessment and management of autoimmune liver diseases. *Eur J Gastroenterol Hepatol.* 2014;26:1065–1072.
13. Rodrigo E, López-Hoyos M, Corral M, et al. ImmuKnow as a diagnostic tool for predicting infection and acute rejection in adult liver transplant recipients: a systematic review and meta-analysis. *Liver Transpl.* 2012;18:1245–1253.
14. Bubak ME, Porayko MK, Krom RA, Wiesner RH. Complications of liver biopsy in liver transplant patients: increased sepsis associated with choledochojejunostomy. *Hepatology.* 1991;14:1063–1065.
15. Regev A, Berho M, Jeffers LJ, et al. Sampling error and intraobserver variation in liver biopsy in patients with chronic HCV infection. *Am J Gastroenterol.* 2002;97:2614–2618.
16. Aran PP, Bissel MG, Whitington PF, Bostwick DG, Adamac T, Baker AL. Diagnosis of hepatic allograft rejection: role of liver biopsy. *Clin Transplant.* 1993;7:475–481.
17. Coffin CS, Burak KW, Hart J, Gao Z. The impact of pathologist experience on liver transplant biopsy interpretation. *Mod Pathol.* 2006;19:832–838.
18. Clark PM, Flores G, Evdokimov NM, et al. Positron emission tomography probe demonstrates a striking concentration of ribose salvage in the liver. *Proc Natl Acad Sci USA.* 2014;111:E2866–E2874.
19. Evdokimov NM, Clark PM, Flores G, et al. Development of 2-deoxy-2-[^{18}F] fluororibose for positron emission tomography imaging liver function in vivo. *J Med Chem.* 2015;58:5538–5547.
20. Salas JR, Chen BY, Wong A, et al. Non-invasive imaging of drug-induced liver injury with ^{18}F-DFA PET. *J Nucl Med.* March 1, 2018 [Epub ahead of print].
21. Laing RE, Nair-Gill E, Witte ON, Radu CG. Visualizing cancer and immune cell function with metabolic positron emission tomography. *Curr Opin Genet Dev.* 2010;20:100–105.
22. Radu CG, Shu CJ, Shelly SM, Phelps ME, Witte ON. Positron emission tomography with computed tomography imaging of neuroinflammation in experimental autoimmune encephalomyelitis. *Proc Natl Acad Sci USA.* 2007;104:1937–1942.
23. Radu CG, Shu CJ, Nair-Gill E, et al. Molecular imaging of lymphoid organs and immune activation by positron emission tomography with a new [^{18}F]-labeled 2′-deoxycytidine analog. *Nat Med.* 2008;14:783–788.
24. Nair-Gill E, Wiltzius SM, Wei XX, et al. PET probes for distinct metabolic pathways have different cell specificities during immune responses in mice. *J Clin Invest.* 2010;120:2005–2015.
25. Brewer S, McPherson M, Fujiwara D, et al. Molecular imaging of murine intestinal inflammation with 2-deoxy-2-[^{18}F]fluoro-D-glucose and positron emission tomography. *Gastroenterology.* 2008;135:744–755.
26. Brewer S, Nair-Gill E, Wei B, et al. Epithelial uptake of [^{18}F]1-(2′-deoxy-2′-arabinofuranosyl) cytosine indicates intestinal inflammation in mice. *Gastroenterology.* 2010;138:1266–1275.
27. de Paula Faria D, Vlaming MLH, Copray SCVM, et al. PET imaging of disease progression and treatment effects in the experimental autoimmune encephalomyelitis rat model. *J Nucl Med.* 2014;55:1330–1335.
28. Maya Y, Werner RA, Schütz C, et al. ^{11}C-methionine PET of myocardial inflammation in a rat model of experimental autoimmune myocarditis. *J Nucl Med.* 2016;57:1985–1990.
29. Terry SYA, Koenders MI, Franssen GM, et al. Monitoring therapy response of experimental arthritis with radiolabeled tracers targeting fibroblasts, macrophages, or integrin αvβ3. *J Nucl Med.* 2016;57:467–472.
30. Ishimori T, Saga T, Mamede M, et al. Increased ^{18}F-FDG uptake in a model of inflammation: concanavalin A-mediated lymphocyte activation. *J Nucl Med.* 2002;43:658–663.
31. Tsuji AB, Morita M, Li X-K, et al. ^{18}F-FDG PET for semiquantitative evaluation of acute allograft rejection and immunosuppressive therapy efficacy in rat models of liver transplantation. *J Nucl Med.* 2009;50:827–830.
32. Collins J, Waldmann CM, Drake C, et al. Production of diverse PET probes with limited resources: 24 ^{18}F-labeled compounds prepared with a single radiosynthesizer. *Proc Natl Acad Sci USA.* 2017;114:11309–11314.
33. Blom KG, Qazi MR, Matos JBN, Nelson BD, DePierre JW, Abedi-Valugerdi M. Isolation of murine intrahepatic immune cells employing a modified procedure for mechanical disruption and functional characterization of the B, T and natural killer T cells obtained. *Clin Exp Immunol.* 2009;155:320–329.
34. Gantner F, Leist M, Lohse AW, Germann PG, Tiegs G. Concanavalin A-induced T-cell-mediated hepatic injury in mice: the role of tumor necrosis factor. *Hepatology.* 1995;21:190–198.
35. Phelps ME. Positron emission tomography provides molecular imaging of biological processes. *Proc Natl Acad Sci USA.* 2000;97:9226–9233.
36. Toy G, Austin WR, Liao H-I, et al. Requirement for deoxycytidine kinase in T and B lymphocyte development. *Proc Natl Acad Sci USA.* 2010;107:5551–5556.
37. Jacobs SR, Herman CE, Maciver NJ, et al. Glucose uptake is limiting in T cell activation and requires CD28-mediated Akt-dependent and independent pathways. *J Immunol.* 2008;180:4476–4486.
38. Agranoff BW, Brady RO. Purification and properties of calf liver ribokinase. *J Biol Chem.* 1956;219:221–229.
39. Clark PM, Ebiana VA, Gosa L, Cloughesy TF, Nathanson DA. Harnessing preclinical molecular imaging to inform advances in personalized cancer medicine. *J Nucl Med.* 2017;58:689–696.
40. Sass G, Heinlein S, Agli A, Bang R, Schümann J, Tiegs G. Cytokine expression in three mouse models of experimental hepatitis. *Cytokine.* 2002;19:115–120.

41. Murphy JM, Armijo AL, Nomme J, et al. Development of new deoxycytidine kinase inhibitors and noninvasive in vivo evaluation using positron emission tomography. *J Med Chem.* 2013;56:6696–6708.
42. Czaja AJ. Challenges in the diagnosis and management of autoimmune hepatitis. *Can J Gastroenterol.* 2013;27:531–539.
43. Dyson JK, Webb G, Hirschfield GM, et al. Unmet clinical need in autoimmune liver diseases. *J Hepatol.* 2015;62:208–218.
44. Staatz CE, Tett SE. Clinical pharmacokinetics and pharmacodynamics of tacrolimus in solid organ transplantation. *Clin Pharmacokinet.* 2004;43:623–653.
45. Jusko WJ, Piekoszewski W, Klintmalm GB, et al. Pharmacokinetics of tacrolimus in liver transplant patients. *Clin Pharmacol Ther.* 1995;57:281–290.
46. Lampen A, Christians U, Guengerich FP, et al. Metabolism of the immunosuppressant tacrolimus in the small intestine: cytochrome P450, drug interactions, and interindividual variability. *Drug Metab Dispos.* 1995;23:1315–1324.
47. Zarrinpar A, Lee D-K, Silva A, et al. Individualizing liver transplant immunosuppression using a phenotypic personalized medicine platform. *Sci Transl Med.* 2016;8:333ra49.
48. Shin E-C, Sung PS, Park S-H. Immune responses and immunopathology in acute and chronic viral hepatitis. *Nat Rev Immunol.* 2016;16:509–523.
49. Bengsch B, Johnson AL, Kurachi M, et al. Bioenergetic insufficiencies due to metabolic alterations regulated by the inhibitory receptor PD-1 are an early driver of CD8(+) T cell exhaustion. *Immunity.* 2016;45:358–373.
50. Shu CJ, Campbell DO, Lee JT, et al. Novel PET probes specific for deoxycytidine kinase. *J Nucl Med.* 2010;51:1092–1098.
51. Ho DH. Distribution of kinase and deaminase of 1-beta-D-arabinofuranosylcytosine in tissues of man and mouse. *Cancer Res.* 1973;33:2816–2820.
52. Schwarzenberg J, Radu CG, Benz M, et al. Human biodistribution and radiation dosimetry of novel PET probes targeting the deoxyribonucleoside salvage pathway. *Eur J Nucl Med Mol Imaging.* 2011;38:711–721.
53. Kim W, Le TM, Wei L, et al. [^{18}F]CFA as a clinically translatable probe for PET imaging of deoxycytidine kinase activity. *Proc Natl Acad Sci USA.* 2016;113:4027–4032.
54. Barrio MJ, Spick C, Radu CG, et al. Human biodistribution and radiation dosimetry of ^{18}F-clofarabine, a PET probe targeting the deoxyribonucleoside salvage pathway. *J Nucl Med.* 2017;58:374–378.